## ORIGINAL RESEARCH



# Green synthesis of cellulose graft copolymers for anion exchange water purification

Steve C. Schmal<sup>®</sup> · Raghav Dosi<sup>®</sup> · Adam Fessler<sup>®</sup> · Carly Kwiatkowski<sup>®</sup> · Abhispa Sahu<sup>®</sup> · Jordan C. Poler<sup>®</sup>

Received: 7 April 2023 / Accepted: 14 September 2023 / Published online: 11 October 2023 © The Author(s), under exclusive licence to Springer Nature B.V. 2023

Abstract A cellulose graft copolymer (cellulose nanoresin) was synthesized by the all-aqueous functionalization of cellouronic acid with poly (vinyl benzyl trimethyl ammonium chloride) (poly(vbTMAC)). Cellulose was oxidized using the highly reported 2,2,6,6-tetramethylpiperidine-1-oxy (TEMPO)-mediated selective C-6 oxidation reaction. Fischer-Speier esterification of cellouronic acid was used to graft poly(vbTMAC) to the cellulosic backbone in a facile click-like mechanism. Synthesis of cellulose nanoresin was confirmed using dynamic light scattering and zeta potential measurements. Conductometric titration was used to determine the carboxylate content of cellouronic acid and the percent functionalization of the cellulose nanoresin, which was  $1.69 \pm 0.03$  mmol/g and  $61.2 \pm 4\%$ , respectively. Using a disodium fluorescein (NaFL) surrogate adsorbate, the maximum adsorption capacity of CNR was measured to be  $26.8 \pm 1.3$  mg NaFL per gram of CNR with a Langmuir equilibrium binding constant of Ks =  $10.5 \pm 2$  ppm<sup>-1</sup>. When examined as a thin film membrane, a breakthrough study of CNR showed

**Supplementary Information** The online version contains supplementary material available at https://doi.org/10.1007/s10570-023-05519-8.

S. C. Schmal · R. Dosi · A. Fessler · C. Kwiatkowski · A. Sahu · J. C. Poler (⋈) University of North Carolina at Charlotte, 9201, University City Blvd, Charlotte, NC 28223, USA e-mail: jcpoler@uncc.edu

that equilibrium loading was achieved in less than 30 s, and that > 90% of loading occurred in under 5 s. This data suggests that these films can be used as contact resins for anion-exchange water purification. We show in this work that these films maintain > 99% of loading performance over 40 trials of regeneration and reuse, meaning that these films are green and regenerable. Initial testing shows that CNR is effective at the removal of perfluorooctane sulfonate (PFOS) from water to below our limit of detection of 100 ppt.

**Keywords** Water purification  $\cdot$  TEMPO oxidized nanocellulose  $\cdot$  Graft copolymers  $\cdot$  Ion exchange  $\cdot$  Green chemistry

#### Introduction

Cellulose and its derivatives have been used for a wide variety of applications including wastewater treatment (Abouzeid et al. 2019; Sahu et al. 2023), coatings, and tissue engineering (Klemm et al. 2006). The scope of cellulose applications has been extended due to extensive surface modifications of cellulose nanofibrils. Cellulose modification reactions typically involve the esterification or etherification of the sugar hydroxyls. Cellulose ethers have been used as stable thickeners in the form of carboxymethylcellulose (Li et al. 2018; Obele et al. 2021), methylcellulose (Bampidis et al. 2020) and hydroxyethyl- and



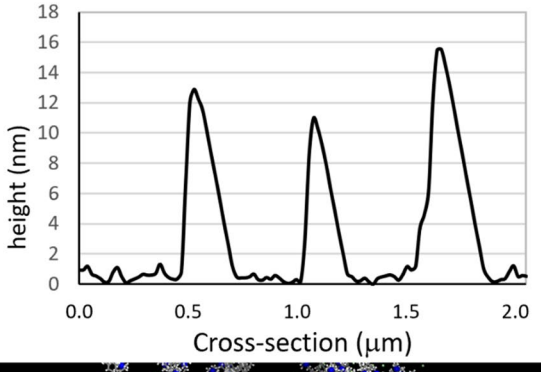
hydroxypropyl-cellulose (Li et al. 2018; Perinelli et al. 2021). Cellulose esterification can introduce a wide range of organic moieties to the polymer chain, allowing for versatile chemical modification. Cellulose esters have been synthesized mainly by inorganic esterification (Camarero Espinosa et al. 2013), Fischer-Speier esterification (Spinella et al. 2016), mechanochemical esterification (Kang et al. 2017), and transesterification (Sèbe et al. 2013) of nanocelluloses. These syntheses lay the groundwork for the acid-catalyzed, all-aqueous synthesis of sustainable cellulose-based water purification materials. Cellulose esters such as cellulose di- and triacetate (Nguyen et al. 2020) and cellulose nitrate (Duan et al. 2016) are typically used as functional films or fibers (Isogai et al. 2018). These chemical modifications to cellulose have also been used to study its use as a scaffold for ion-exchange materials (O'Connell et al. 2008). Crosslinking (Aburabie et al. 2021) and polymer blending of cellulose acetate and poly(methyl methacrylate) (Jois and Bhat 2013) have been studied to increase the ion-exchange capacity of polymer blends, with proton conductivities on the order of  $10^{-2}$  and  $10^{-3}$  S cm<sup>-1</sup>, respectively. Moreover, surface-initiated atom-transfer radical polymerization (SI-ATRP) has been used to graft ionomers onto cellulose fibrils for cellular flocculation studies (Yoshikawa et al. 2022). In our current work, cellulosescaffolded graft copolymers were synthesized with covalently bonded polyelectrolyte branches for use as ion-exchange water purification materials.

Increase in ion-exchange capabilities by surface modification of cellulose has been previously demonstrated by sulfonation (Nikiforova and Kozlov 2011), phosphorylation (Luneva and Ezovitova 2014), and quaternization (Gurgel et al. 2009). These surfacemodified cellulosic materials exhibit increased adsorption properties toward Cu<sup>2+</sup> and Ni<sup>2+</sup>, Fe<sup>2+</sup> and UO<sub>2</sub><sup>2+</sup>, and Cr<sup>6+</sup>, respectively. Isogai et al. work on site-specific oxidation of the primary hydroxyl in cellulose using 2,2,6,6-tetramethylpiperlidine-1-oxyl radical (TEMPO) has enabled a facile click-like methodology for cellulose modification (Isogai and Kato 1998). The synthesis of polyglucouronic acid, or cellouronic acid, has led to applications in flexible electrodes (Lu et al. 2016), antistatic coatings, electrical conductors (Ito et al. 2018), energy storage (Luo et al. 2016) and ion-exchange membranes (Juntadech et al. 2021; Kalia et al. 2014). Cellouronic acid is a commonly used support material for nanofiltration ion-exchange membranes produced by interfacial polymerization of monomer building blocks (Geise et al. 2010). Amidation of these acid groups also enables further synthetic fidelity (Calderón-Vergara et al. 2020). Modified cellulosic materials have been used to produce cation-exchange membranes for the removal of heavy metals such as lead, copper, zinc, nickel, cobalt, cadmium, mercury, iron, and chromium (O'Connell et al. 2008; Sharma et al. 2021).

Oxidized cellulose structures have been used to synthesize copolymers with applications in ionexchange membranes. Singh et al. achieved surface functionalization of poly(acrylic acid) onto regenerated cellulose membranes (Singh et al. 2008). Cellulose nanofiber modification by surface-initiated atom transfer radical polymerization has been used to graft copolymer brushes that have applications in binding and separation of biomolecules, microelectronics, and ultrafiltration (Morits et al. 2017). Though the grafting of cellulose-polyelectrolyte copolymers has been studied, the synthesis of a copolymer using the carboxyl functional groups of TEMPO-oxidized nanocellulose (TONC) and the primary alcohol of an atom transfer radical polymerization (ATRP) initiator is, to our knowledge, novel.

Herein, we report the acid-catalyzed Fischer-Speier esterification using the carboxylated groups of TONC and the primary alcohol group of the HEBIB ATRP initiator to produce a graft bottlebrush copolymer. These materials exhibit anionexchange functionality with applications in water purification as thin film membranes. The structure of these cellulose nanoresins (CNR) is illustrated in the geometry optimized model shown in Fig. 1. Figure 1 (middle panel) is an end on view of this model where poly(vbTMAC)<sub>n=30</sub> polyelectrolyte brushes are grafted to a small cluster of cellulose nanofibers. The cellulose core is 3 nm in diameter and the entire structure is 15 nm in diameter calculated from geometry optimized model). The top panel is the tapping mode atomic force microscope cross-section of these nanofibrils deposited on a silicon substrate (AFM scan shown in figure S9). The average fibril height from representative scans is consistent with the calculated diameter ~ 14 nm. The AFM height data are consistent with high-resolution SEM cross-sectional width data, shown in Fig. 9 and figures S8A-D. The edge on view in Fig. 1 (bottom panel) illustrates the





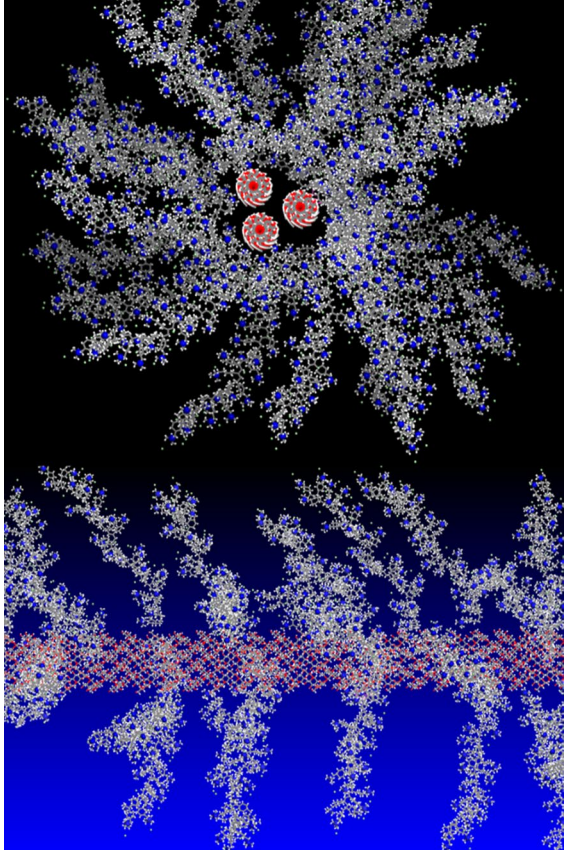


Fig. 1 Molecular Mechanics (Compass force-field) geometry optimized structure of poly(vbTMAC) grafted – cellulose nanofibers. End-on view (middle panel) and Edge view (bottom panel). Tapping mode AFM cross-section of cellulose nanoresin fibril shown in top panel

measured percent functionality of the TONC with polyelectrolyte. As discussed below, 30% of the primary alcohol groups were oxidized and 60% of those were grafted with poly(vbTMAC) so that 18% of glucose subunits are functionalized. We show below that

this morphology leads to high water flux and high analyte loading capacity.

### Materials and methods

Polyelectrolyte synthesis

Poly(vinyl benzyl trimethyl ammonium chloride) (poly(vbTMAC) was synthesized via an aqueous process (Sahu et al. 2020) activators regenerated by electron transfer atom transfer radical polymerization (ARGET-ATRP) mechanism, originally developed by Matyjaszewski (Matyjaszewski et al. 2007). The catalyst was prepared by adding 51.7 µL of a 20.6 mM (1.07 µmol) copper (II) bromide (Arcos, 99+%; Lot #A0344238) solution to 1.000 mL water along with 18.50 mg (63.71 µmol) of tris(2-pyridylmethyl)amine (TPMA) (TCI, >98.0%; Lot #Z8GMO-A). The monomer vinyl benzyl trimethyl ammonium chloride (vbTMAC) (Fisher, 97%; Lot#A0311318) (1.6001 g, 7.557 mmol) was then added along with 30.0 mL of water. The mixture was then sparged with Ar(g) for 20 min to remove oxygen from the reaction vessel, as oxygen would oxidize the copper in the catalyst complex from the Cu<sup>+</sup> to the Cu<sup>2+</sup> state, thereby removing the activator species from the reaction. The ATRP initiator, 2-hydroxyethyl 2-bromo-isobutyrate (HEBIB) (Sigma-Aldrich, 95%, Lot #MKBW2607) was then added (35.5 µL, 252 µmol). The reducing agent, tin(II) 2-ethylhexanoate (Sigma-Aldrich, 92.5–100%, Lot #SLBP5072V) was then added to the reaction vessel (60 μL). The reaction vessel was heated in a 110 °C oil bath with constant stirring under Ar(g) at reflux conditions for 151 h. The polymer solution was purified by centrifugation and dialysis. The concentration of the purified polyelectrolyte solution was determined by solvent evaporation. Typical concentrations were in the range of 10-100 mg/mL.

During the polymerization several 100  $\mu L$  aliquots were taken for subsequent <sup>1</sup> H NMR analysis to quantitatively measure the percent conversion of vbTMAC monomer to polymer. By integrating the doublet at 5.8 ppm chemical shift, which corresponds to one of the vinylic protons, the percent conversion of vbTMAC monomer was calculated. Dimethyl formamide was added to the NMR aliquot as an internal standard (10.00  $\mu L$ ) and then diluted by a factor of 10 into  $D_2O$  and filtered using 0.45  $\mu m$  pore size



nylon Cameo 3 N syringe filters (GE Water & Process Technologies, Catalog No. DDR0400300). Figures S1 and S2 show the 1 H NMR spectra of the vbTMAC monomer and the polymerized product, respectively. Percent conversion was calculated as  $%Conversion = [1 - (S_t/S_0) * 100]$  where  $S_t$  is the integrated signal at 5.8 ppm of the vinylic protons on the vbTMAC monomer (see structure in figure S2) at time t and  $S_0$  is the integrated signal at the start of the polymerization. Once 99% conversion was achieved, the reaction was quenched by allowing air into the reaction vessel and the product was purified by centrifuging at 15,000 RCF for 4 h and then dialyzing against water through a 2 kDa molecular weight cut off cellulose dialysis membrane to remove any remaining monomer and other reagents.

## TEMPO oxidized cellulose synthesis

Oxidation of cellulose was performed using 2,2,6,6-tetramethylpiperidine 1-oxyl (TEMPO) (Sigma-Aldrich, Lot #BCBZ3312). This procedure made use of the well-established synthetic route that selectively targets the C-6 carbon of the D-glucose monosaccharide units (Shibata 2003). In a 50 mL round bottom flask, NaBr (Fischer Scientific, Lot #067787) (0.256 g, 2.49 mmol) and TEMPO (11.64 mg, 74.50 µmol) were dissolved in 25.0 mL of water. Cellulose (Sigma-Aldrich, Lot# MKCJ3230) (0.512 g, 3.21 mmol) was then added, and the pH was adjusted to 10.3 using NaOH. Oxidation was initiated by adding 13.9 mmol of NaOCl(aq) while maintaining the pH using NaOH. The reaction mixture was cooled to 10 °C using an RTE-9 Endocal refrigerated cooling bath and sonicated at 72 W cm<sup>-2</sup> to debundle the cellulose fibers. After 2 h of sonication, the sonicating probe was removed, and the reaction was allowed to continue for 24 h. Ethanol was added to the reaction vessel to quench the oxidation, and the products were centrifuged with ethanol twice and acetone once at 15,000 g at 4 °C for 1 h each. Following each centrifugation, the supernatant liquid was wasted, and the pellet was scraped out. The pellet from the final washing was dried for 24 h in a vacuum oven at 90 °C. The dried pellet was dispersed in 100.0 mL of water and sonicated at 45 W cm<sup>-2</sup> for 20 min. The dispersion was then centrifuged at 100,000 g at 20 °C for 75 min and the supernatant containing the TEMPO-oxidized nanocellulose (TONC) product was collected. The concentration of TONC was determined by solvent evaporation to be 96 mg/L.

#### Characterization of oxidized cellulose

Percent carboxylation of cellulose was determined by conductometric titration. 10.000 mL of TONC was added to 100.0 mL of water and 1.000 mL of 0.1000 N HCl to reduce the pH far below the pKa of acetic acid, ensuring the protonation of all C-6 carboxyl groups in TONC. The initial pH of the solution was 1.29. NaOH (189.3 mM) was added, and the conductivity was monitored using a conductivity probe (Fischer Scientific, AR20 pH/conductivity meter with Acumet Research conductivity probe). Carboxylate content was calculated by dividing the number of moles of NaOH required to neutralize the carboxylate groups of TONC by the mass of TONC.

Synthesis and characterization of cellulose nanoResin (CNR)

CNR synthesis was optimized by first experimenting with alternative synthetic methods for TONC synthesis. High-pressure homogenization (HPH) was used during the oxidation reaction to increase the surface area of the cellulose reagent. For this reaction, 20.00 g cellulose was added to 2.000 L of DI water and 9.8563 g NaBr was dissolved in the mixture. 20.0 mL of 171.8 mM NaOH was then added, and the pH was measured to be approximately 10 using universal indicator strips. 450 mg of TEMPO was then added to the reaction mixture, and 175 mL of bleach (8.25%) was then introduced to allow oxidation to begin. The reaction mixture was passed through the highpressure homogenizer 12 times at 8000 PSI, then 4 more times at 14,000 PSI. The HPH TONC was then centrifuged and purified using ethanol and acetone as described above. A second sample of TONC was prepared by sonicating HPH TONC for 2 h at 10 W<sub>RMS</sub> before centrifuging and purifying the sample. A third TONC sample was prepared by sonication only, while maintaining the mixture at pH = 10 during the oxidation reaction. For this reaction, 1.023 g cellulose was added to 50.0 mL DI water along with 514.1 mg NaBr and 23.6 mg TEMPO. 500.0 µL of 171.8 mM NaOH was then added and the pH was measured to be 10.19. The reaction was started by adding 17.0 mL of bleach (8.25%), after which the pH was measured to be about



4 using universal indicator strips. 6.000 mL of 171.8 mM NaOH was then added, and the pH was measured to be approximately 10. The pH of the reaction was measured every 15 min for 2 h and did not change for the entirety of the reaction. The reaction mixture was sonicated for 2 h at 10 W<sub>RMS</sub> before subsequent quenching and purification. The carboxylate content of the three TONC samples (HPH only, HPH+sonicated, and sonicated, pH controlled TONC) were measured by conductometric titration. IR spectra of the TONC, CNR, and other reagents were acquired by ATR FT-IR using a PerkinElmer Spectrum 100 FT-IR spectrometer with attenuated total reflectance (ATR) crystal assembly. Spectral range was 4000–650 cm<sup>-1</sup> at 2 cm<sup>-1</sup> resolution, and typically 16 scans. CNR solutions were sonicated in 4 M NaCl(aq) to remove any physiosorbed polymer. The purified CNR solution was filtered onto a  $0.22\ \mu m$  polypropylene membrane, rinsed with 4 M NaCl(aq) and then ~200 mL of deionized water to wash away any polymer that was not covalently bound to the cellulose nanofibrils.

Esterification of sonicated, pH controlled TONC was carried out four times with varying mole fractions to determine the stoichiometry of the reaction. Each reaction was performed under reflux conditions for 72 h using 10.00 mL of 192 mg L<sup>-1</sup> TONC and 100.0 µL concentrated HCl. The carboxylate content of sonicated, pH controlled TONC was determined by conductometric titration to be  $1.69 \pm 0.03$  mmol/g (Fig. 3).  $Poly(vbTMAC)_{n=30}$  30-mer, (14.8 mg mL<sup>-1</sup>, molar mass = 6563 Da) was added using volumes of 137.0 μL, 685.0 μL, 1.370 mL, and 2.740 mL to reach mole fractions of 0.0950, 0.476, 0.952, and 1.90, respectively. Following the completion of the esterification reactions, each product was filtered with 0.2 micron pore size, 13 mm polypropylene filters. PF was then determined for each product using conductometric titration. During each titration, 2 mL of CNR was mixed with 100 mL of water and 2.000 mL of 0.1000 N HCl and then titrated with 17.18 mM NaOH. Carboxylate content of each product was calculated from the moles of NaOH required to neutralize the carboxyl groups, and PF was calculated for each esterification.

Typical TONC esterification reaction conditions were,  $5.000\,\text{mL}$  of 192 mg/L TONC was added to  $1.370\,\text{mL}$  poly(vbTMAC)<sub>n=30</sub> (14.8 mg/mL) along with  $100.0\,\mu\text{L}$  concentrated HCl. Reaction times of  $1.0\,\text{h}$ ,  $4.0\,\text{h}$ ,  $6.0\,\text{h}$ ,  $14.0\,\text{h}$ ,  $17.0\,\text{h}$ , and  $24.0\,\text{h}$  were

performed and characterized. PF for each reaction was determined by conductometric titration. Each purified CNR was characterized by Dynamic Light Scattering (DLS) and zeta potential, using a Malvern DLS Zetasizer. Pristine commercial cellulose or CNR was dispersed in water and sonicated at 45 W cm<sup>-2</sup> for 3 h. The dispersion was then centrifuged at 3,000 g at 20 °C for 20 min. The transparent solution was then diluted in 0.1 mM potassium chloride solution for DLS analysis. DLS accuracy was determined using Duke Scientific NIST traceable  $92 \pm 3.7$  nm polymer nanospheres in 0.1 mM KCL. Zeta potential accuracy was determined using the Malvern Zeta Potential Standard  $-42 \pm 4.2$  mV solution. CNR morphology was also measured using a LEO 1550 field emission scanning electron microscope (SEM) and a Digital Instruments NanoScope tapping mode atomic force microscope (AFM). Samples were deposited onto silicon chips that were first cleaned using a piranha etch solution (3:1 sulfuric acid/30% hydrogen peroxide). 1.000 mL of a 25.75 mg/L aqueous CNR solution was sonicated at 5  $W_{RMS}$  for ~1 min. The clean Si chip was added to the solution and incubated for 45 min. The sample was then dried with  $N_2$  gas.

## Characterization of adsorption capacity and kinetics

The adsorption capacity of CNR was determined using UV-Vis spectroscopy. Fluorescein disodium salt (NaFL) (Sigma-Aldrich Lot #: BCBR1213V, CAS: 518-47-8) was used as a surrogate adsorbate for natural organic matter acids. 200 µL of 186 mg/L CNR (37.2 µg) was incubated for 30 min in dilute NaFL solutions. Initial NaFL concentrations ranged from 0.252 to 3.18 ppm (see table S1 for data). Following incubation, each sample was filtered using 0.45 µm pore size nylon filters. The amount of NaFL adsorbed per gram of CNR was calculated by measuring the absorbance of the mixture at 491 nm before and after incubation and filtration. 30.00 µL of 171.8 mM NaOH was added to 2.000 mL solution before measuring the absorbance at 491 nm. Because sodium fluorescein absorbs most strongly in the deprotonated form (pH>10), with an extinction coefficient of  $\varepsilon_{491} = 0.238 \text{ ppm}^{-1} \text{ cm}^{-1}$ , low concentrations of effluent NaFL could be measured to a limit of detection of 4 ppb. Adsorption kinetics were measured by incubation of CNR in a NaFL(aq) solution.





**Fig. 2** CNR film deposited on an MCE support. Membrane flux is measured (left). Breakthrough data acquired by passing NaFL through the film until the  $C/C_o=1.0$ . Yellow fluorescein dye of CNR is shown. (right). Regenerated films are again white

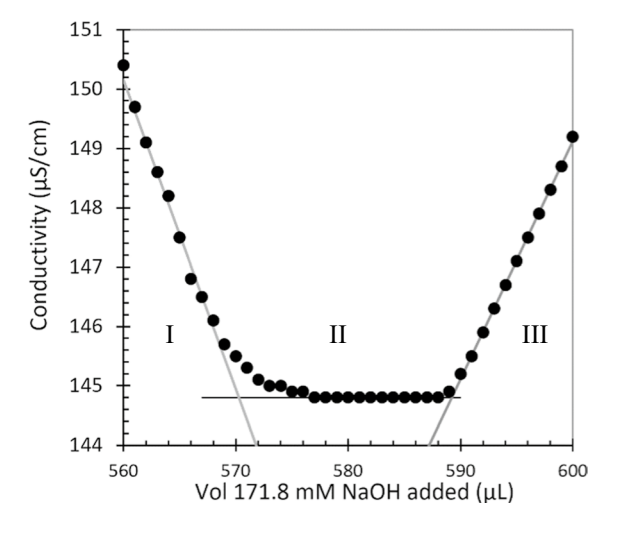


**Fig. 3** Conductometric titration data. 10.000 mL 192 mg/L sonicated pH controlled TONC, titrated with 0.1718 M NaOH.  $18.9\pm0.2~\mu\text{L}$  of NaOH were required to neutralize the weak acid carboxylated groups

All samples started with an initial concentration  $C_o = 3.70$  ppm and pH between 6 and 7.5. After a short incubation time the CNR was removed by filtration through a 0.45  $\mu$ m pore size nylon filter, and the concentration of remaining fluorescein was measured by UV-Vis spectroscopy. Control study of the same NaFL solution pushed through a nylon filter resulted in no color change on the filter itself and negligible < 1% non-specific binding to the filter.



Membrane flux experiments were conducted on HPH TONC and CNR. For these experiments, CNR sample material was deposited onto 47 mm diameter, 0.1 µm pore size mixed cellulose ester (MCE) filters such that the areal density was 1.345 mg cm<sup>-2</sup> and water flux was measured in L m<sup>-2</sup> h<sup>-1</sup> bar <sup>-1</sup>. Breakthrough curve data were collected by passing 3.965 ppm NaFL through the film, and membrane water flux data was taken before and after adsorption of NaFL, shown in Fig. 2. The regenerable nature of these membranes was tested by passing 600 µL of 190 mg/L CNR (114 µg) through a 25 mm diameter 0.2 µm pore size MCE film. NaFL was then pushed through the film using a 10 mL syringe, and the concentration of NaFL was measured before and after adsorption. Following adsorption, 4 M brine (approximately 20 mL) was pushed through the membrane to desorb the NaFL until the concentration of desorbed analyte was below the UV-Vis detection limit of 30 ppb. DI water (approximately 60 mL) was then pushed through the membrane to remove the sodium and chloride ions until the conductivity measured by a Pharmacia Biotech conductivity flow cell monitor was  $< 1 \mu S cm^{-1}$ . Subsequent cycles were then performed by pushing NaFL through the membrane, followed by brine and water up to 40 cycles without any performance degradation. A control experiment passing the same amount of NaFL through an MCE membrane without any CNR showed no color change to the MCE and negligible, < 1% non-specific adsorption of the analyte.

## Results and discussion

Three methods of cellulose oxidation were tested to maximize the carboxylate content of the fibrils. All these samples were purified by centrifugation. Carboxylate content of TONC and CNR was determined by conductometric titration. Onset and endset values of the titrant were determined by the intersection of the linear regression fits from region I and II (onset) and regions II and III (endset). As shown in Fig. 3, titration of 10.00 mL of 192 mg/L pH controlled TONC (1.92 mg, 10.6  $\mu$ mol glucose subunits) required 18.9 $\pm$ 0.2  $\mu$ L of 0.1718 M NaOH (3.25 $\pm$ 0.04  $\mu$ mol) to completely neutralize the C-6



carboxylate groups. This result indicates that 30.7% of all C-6 hydroxyl groups were carboxylated during the oxidation reaction, giving a carboxylate content of  $1.69\pm0.03$  mmol g<sup>-1</sup>. Figure S6 illustrates the conductometric titrations of the other oxidized cellulose samples. The neutralization of the acetate groups in 10.00 mL each of HPH only, HPH+sonicated, and sonicated, pH controlled TONC required  $7.85\pm0.2$  µL,  $10.2\pm0.5$  µL, and  $18.9\pm0.2$  µL of 171.8 mM NaOH, giving carboxylate contents of  $1.11\pm0.03$  mmol g<sup>-1</sup>,  $1.29\pm0.07$  mmol g<sup>-1</sup>, and  $1.69\pm0.03$  mmol g<sup>-1</sup> respectively. For subsequent CNR synthesis esterification reactions, the TONC sample with the highest carboxylate content, sonicated – pH controlled TONC, was used.

IR spectra of the TONC, CNR, polymer, and starting reagents are shown in figure S7A. The band of peaks in the range 3025–2830 cm<sup>-1</sup> describe C-H stretching from the vinyl alkene and alkane bonds from the polyelectrolyte. The three peaks found in pure monomer are centered on a strong peak at 3015 cm<sup>-1</sup> characteristic of the vinyl C-H (Johnson et al. 2016). Upon polymerization, peak shifts by 95 cm<sup>-1</sup> to 2920 cm<sup>-1</sup> due to the change in aromatic character and the intramolecular interactions in the polyelectrolyte chain (red line). The band of these absorptions shifts again, by  $\sim 9 \text{ cm}^{-1}$  when the polymers are covalently attached to the cellulose fibrils due to additional steric crowding in the final CNR product (black line). The central peak shifts to 2913 cm<sup>-1</sup> as shown in the zoomed in spectra in figure S7B. There is only a weak and broad absorption found in the TONC spectra (blue line). As described in the methods section, the CNR films were purified so that the only polymer present was covalently bound to the TONC fibrils through the esterification reaction. The initiator group used to react with the carboxylic acid on the TONC also contains an ester group. The spectra of the initiator, 2-hydroxyethyl 2-bromo-isobutyrate (HEBIB), is shown in figure S7C (magenta line) where the sharp and strong absorption at 1730 cm<sup>-1</sup> is characteristic of the C=O stretching of an ester. When the initiator is in the n = 30 polymer (see Scheme 1 above) we do not observe this band, nor do we see the 1730 cm<sup>-1</sup> band in the CNR for the same reason. There is only one ester C=O in the 6330 Da polymer strand or the even larger CNR bottlebrush. Also, the ester is very sterically crowded, and possibly bridged by bound water, which will shift the band to lower energies.

Dynamic light scattering was used to confirm debundling of the cellulose nanofibrils. Figure S3a and S3b show the particle size as hydrodynamic diameter for cellulose and TONC, respectively. The hydrodynamic diameter of the cellulose fibrils decreased from 142.1 nm to 30.08 nm after oxidation, indicating successful debundling of the cellulose nanofibrils. The zeta potential of cellulose was also measured before and after oxidation. As shown in figure S4, the zeta potential was determined to be -0.10 mV and -27.7 mV for cellulose and TONC, respectively. The negative surface charge of the TONC product is indicative of successful oxidation when compared to the relatively neutral surface charge of the pristine cellulose.

The hydrodynamic diameter and zeta potential were measured for CNR. Results are shown in figure S5. An increased size of 207.9 nm suggests that TONC was successfully functionalized with  $poly(vbTMAC)_{n=30}$ . Additionally, a positive surface charge of +17.3 mV further supports the introduction of quaternary ammonium cations to the cellulose backbone.

The percent functionalization (PF) of the cellulose fibril scaffold was determined by conductometric titration of the bottlebrush product. 2.000 mL (0.299 mg TONC, 1.65 µmol) of CNR was added to 100 mL of water along with 2.00 mL of 0.1000 N HCl, bringing the pH to 2.93. The mixture was then titrated with 17.18 mM NaOH. After neutralization of the excess HCl (region I), the C-6 carboxyl groups remaining after the esterification reaction required  $11.19 \pm 0.18 \mu L (0.1922 \mu mol)$  of 17.18 mM NaOH (Fig. 4). This result indicates a residual carboxylate content of 0.775 mmol/g of the CNR product. From the initial carboxylate content of the TONC and the result in Fig. 4, the PF was calculated to be  $61.2 \pm 4\%$ . Since 30.7% of all cellulose glucose subunits were oxidized and 61.2% of those were functionalized with the polyelectrolyte  $(poly(vbTMAC)_{n=30})$  then 18.8% of all glucose subunits were functionalized with a polyelectrolyte strand, as illustrated in Fig. 1). Each strand has about n=30 quaternary ammonium salt binding sites. Therefore, the theoretical binding capacity of this anion exchange material is 27 meq/g TONC.

The percent functionalization of the sonicated pH controlled TONC was measured as a function of the mole ratio of poly(vbTMAC)<sub>n=30</sub> to TONC carboxyl



Scheme 1 Coupling of poly(vbTMAC) to TONC via acid-catalyzed Fischer-Speier esterification. HEBIB initiator is coupled to the carboxyl group of TONC by reaction with its primary hydroxyl group

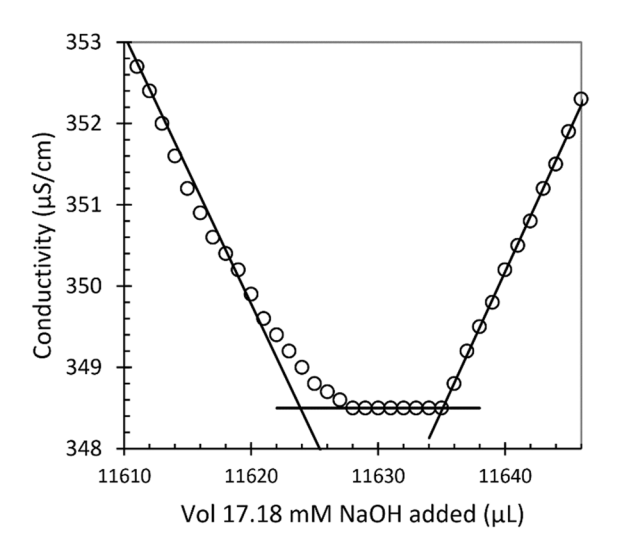


**Fig. 4** Conductometric titration of CNR using 17.18 mM NaOH. Neutralization of carboxylated C-6 groups in 299  $\mu$ g of CNR required 0.1922  $\mu$ mol NaOH. 61.2% of all carboxylates were functionalized with polymer stands

groups during esterification. TONC esterification was performed for 72 h each using mole fractions of 0.1, 0.5, 1, and 2. Conductometric titration data for each product are shown in figure S10. As shown in Fig. 5, a maximum PF of  $61.2 \pm 4\%$  was achieved when using a mole ratio of 2:1 poly(vbTMAC) to TONC carboxyl groups. The effective hydrodynamic diameter of the n=30 polyelectrolyte strands is 1.7 nm (Sahu et al. 2018). The distance between the C-6 carbons of the D-glucose units is ~0.6 nm and 19% of them are functionalized so there is ~3 nm between functionalization sites. Aqueous esterification does not typically proceed to completion, so there does not appear to be a steric constraint on longer polyelectrolyte functionalization which will be studied in future works.

For each of the syntheses shown in Fig. 5 the samples were purified and the bottle-brush assemblies were analyzed by DLS and zeta potential. As



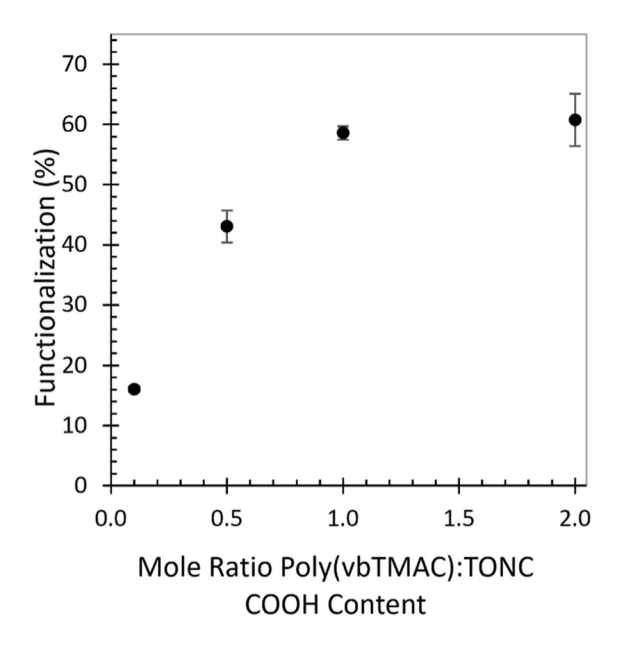


**Fig. 5** Percent functionalization as a function of the mole ratio of poly(vbTMAC) $_{n=30}$  to TONC carboxyl groups during esterification. Maximum percent functionalization was achieved at a 2:1 mol ratio

shown in Fig. 6 (blue square) the hydrodynamic diameter increased from 30 nm for un-functionalized TONC to 200 nm for fully functionalized TONC.

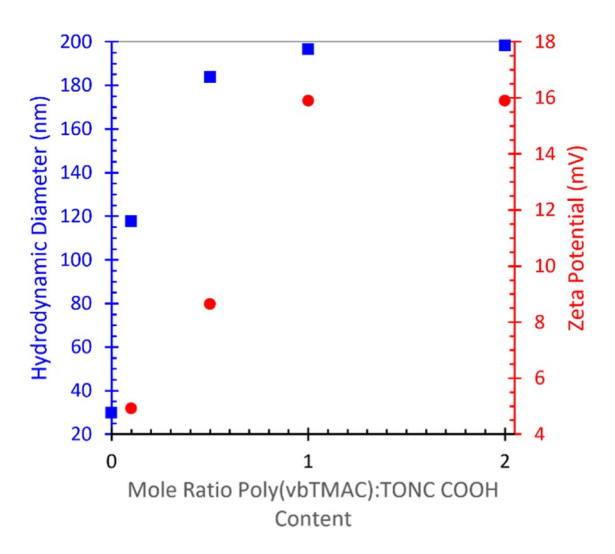


**Fig. 6** Hydrodynamic diameter (blue square) and positive zeta potential (red circle) as a function of the mole ratio of poly(vbTMAC) $_{\rm n=30}$  to TONC carboxyl groups during acid-catalyzed esterification. Maximum size of 198.2 nm and surface charge of +15.9 mV was achieved at a 2:1 mol fraction

These data are consistent with the geometry optimized structure in Fig. 1. Each polyelectrolyte strand is partially extended, and the hydrodynamic diameter is calculated from the Stokes-Einstein relation by assuming a spherically diffusing particle. When we assume a flexible rod model with typical length L=600 nm and width w=15 nm, we can calculate an effective hydrodynamic diameter (Nair et al. 2008)  $D_h = L/(ln(L/w) + 0.32) = 150$  nm, which is consistent with our experimentally determined value. The assembly's zeta potential was measured as the degree of functionalization increased. The zeta potential of the un-functionalized TONC was -27.7 mV due to the deprotonated nature of the carboxyl groups at neutral pH. As the positively charged polyelectrolyte was functionalized to the cellulose scaffold the zeta potential became positive and increased to +16 mV when the stoichiometric ratio was largest, as shown in Fig. 6 (red circles). These assemblies form stable dispersions in water and form continuous crack-free membrane films.

Kinetics of the TONC esterification was studied in an aqueous reaction under reflux. Data shown in Fig. 7 are from the reaction of poly(vbTMAC) $_{\rm n=30}$  strands with sonicated pH controlled TONC scaffolding using a 2:1 molar ratio of strands to carboxyl groups, as a function of time. The data were fitted to a second order kinetics model with equilibrium

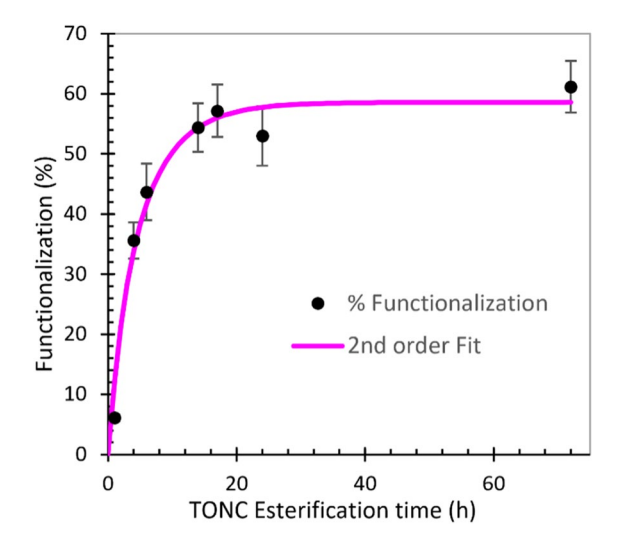


**Fig. 7** Percent functionalization of poly(vbTMAC)<sub>n=30</sub> to TONC (2:1 mol ratio) as a function of time. The data are fitted to a second order A+B in equilibrium with P, kinetic model



 $[poly(vbTMAC)] + [TONC\ carboxyl] \rightleftharpoons [CNR]$ . The fitted forward rate constant  $k_1 = 0.0014\ h^{-1}\%^{-1}$  with an apparent equilibrium concentration  $[CNR]_{eq} = 59\%$ 

For each CNR product shown in Fig. 7, the effective diameter and zeta potential were measured and are shown in Fig. 8. As the percent functionalization, as determined by conductometric titration, increases so does the hydrodynamic diameter from 30 to 198.2 nm due to the conformal coating of polyelectrolyte brushes along the cellulose nanofibril scaffold. Each strand includes n=30 positively charged quaternary ammonium groups leading to the increased zeta potential of the assemblies. Native cellulose has a zeta potential near zero, the sonicated pH controlled TONC has a zeta potential of -27.7 mV and the fully functionalized cellulose nanoresin CNR has a zeta potential of +15.9 mV. These stable dispersed assemblies behave as strong base anion exchange resins.

Structural characterization of the CNR was done using scanning electron microscopy and atomic force microscopy. Representative SEM image of the CNR fibrils on a silicon chip are shown in Fig. 9. A more detailed SEM analysis is shown in figures S8A-D. Some nanoresin fibrils are aggregated or overlapping while the thinnest, unbundled fibrils, are clearly resolved. The cross-sectional width of

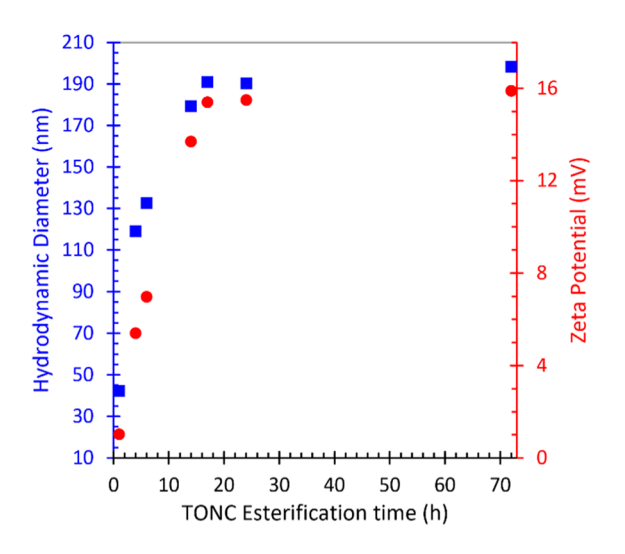


**Fig. 8** Hydrodynamic diameter (blue square) and positive zeta potential (red circle) as a function of esterification time of  $\operatorname{poly}(vbTMAC)_{n=30}$  to TONC carboxyl groups for 2:1 mol ratio initial condition

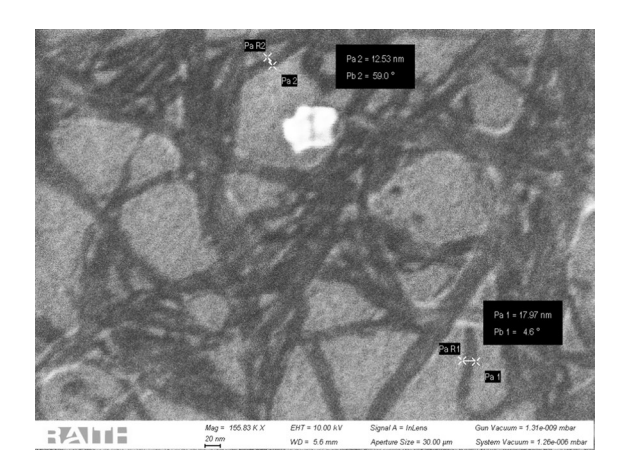


**Fig. 9** SEM micrograph of CNR deposited on clean silicon surface. Individual and overlapping nanoresin fibrils are clearly resolved. The thinnest, unbundled fibrils have a cross-section of ~15 nm. (20 nm scale bar)

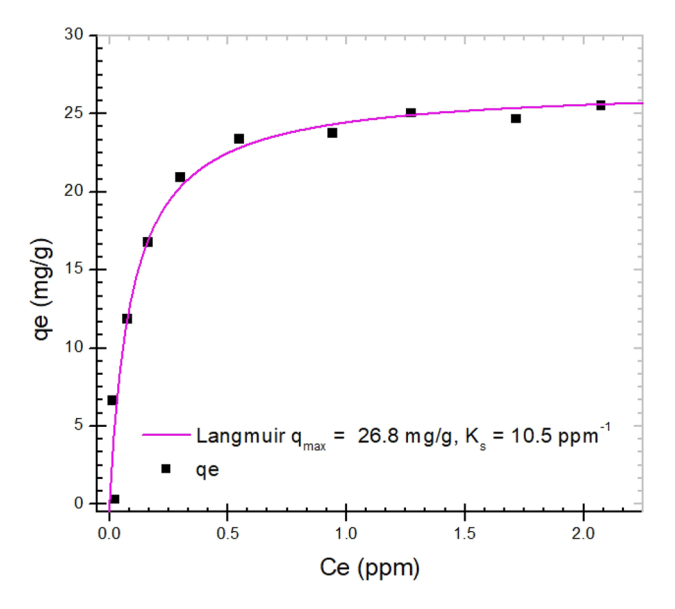
these unbundled fibrils is  $\sim 15$  nm wide. This is consistent with the cross-sectional height data shown in the tapping mode AFM of Fig. 1 (top panel). Tapping mode AFM of the same SEM sample is shown in figure S9.

Adsorption kinetics and equilibrium adsorption capacity of the CNR assemblies and films was determined using a NaFL surrogate adsorbate. Adsorption isotherms, such as those shown in Fig. 10, were measured by adding 200 µL (37.2 µg) of 186 mg/L CNR to NaFL aqueous solutions of varying initial concentrations C<sub>i</sub> such that the total volume of each sample was 2.000 mL. Each sample was allowed to incubate for 30 min. The initial and equilibrium concentration of NaFL for each of the seven samples can be found in table S1 in the Electronic Supplementary Materials (ES) section. The equilibrium concentration of NaFL was calculated by measuring the absorbance at 491 nm. For NaFL,  $\varepsilon_{491} = 0.238 \text{ ppm}^{-1} \text{ cm}^{-1}$  and the limit of detection is 4 ppb. Adsorption capacity qe was calculated as mg of adsorbed fluorescein anion per gram of CNR. Figure 10 shows the equilibrium loading capacity (q<sub>e</sub>) of CNR as a function of equilibrium concentration (C<sub>e</sub>). These data were fitted to the Langmuir adsorption isotherm.

solid line in Fig. 10. These data indicate that the maximum adsorption capacity  $(q_{max})$  of CNR is  $26.8\pm1.3$  mg NaFL per gram of CNR and the Langmuir equilibrium binding constant is  $K_s=10.5\pm2$  ppm<sup>-1</sup>. The data were also fitted to the Freundlich



Fig. 10 Adsorption isotherm data of surrogate absorber NaFL bound to CNR in an aqueous dispersion. Incubation time of 30 min far exceeds equilibrium binding time  $t_e$ . Data are fitted to a Langmuir model (solid line) and  $q_{max}$  and  $K_s$  are determined



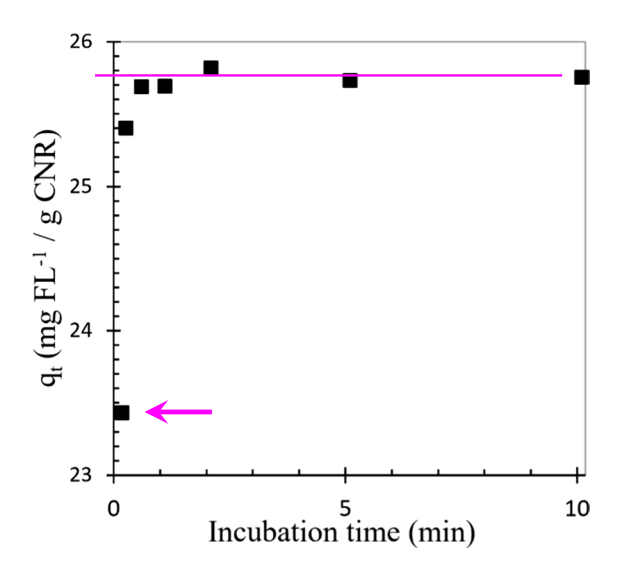


**Fig. 11** Adsorption kinetics data of surrogate absorber NaFL bound to CNR in an aqueous dispersion. Initial NaFL concentration is held constant. The CNR adsopbed > 90% of its maximum value (line) in less than 5 s (arrow)

and BET isotherms. The Langmuir function gave the best statistical fit to the data (Alston et al. 2015).

In Fig. 11 the loading  $q_t$  (mg fluorescein anion per gram CNR) is plotted versus time. The equilibrium binding  $q_e = 25.8$  mg/g is reached in less than 30 s. Moreover, >90% of the binding occurs in less than 5 s of incubation (first data point in Fig. 11). These materials behave like "contact" resins whereas

there is no need for diffusive transport of the analyte into the polymer. The binding sites of the brush-like assemblies are easily accessible. The CNR performance as a membrane film also exhibits this fast, yet strong binding.

The performance of CNR as thin-film adsorbent membranes was tested by measuring membrane water flux and breakthrough curve data. The membrane water flux of HPH TONC and CNR was measured to be 281 and 783 L m<sup>-2</sup> h<sup>-1</sup> bar <sup>-1</sup>, when tested using 0.1 µm pore size, 47 mm MCE films with areal densities of 1.412 and 1.345 mg cm<sup>-2</sup>, respectively. When a dispersion of TONC aggregates during film formation, the fibrils become compact and decrease the water flux through the membrane. When the polyelectrolyte brushes extend out from the fibrils, the film can form a more open structure such that water can flow more freely while the analyte must take a tortuous path through a mesh of binding sites. Simultaneously maximizing the water flux, binding capacity, and binding speed is a central aim of this translational research. Breakthrough curve data for CNR adsorbing NaFL are shown in Fig. 12. A solution of aqueous NaFL, with initial concentration  $C_0 = 1.9$  ppm and pH between 6 and 7.5, is pushed through the membrane at a flow rate of 46 mL/min and the concentration of analyte, C, passing through the membrane was measured as a function of effluent volume V<sub>eff</sub>. These data are modeled using the Thomas equation for dynamic adsorption,



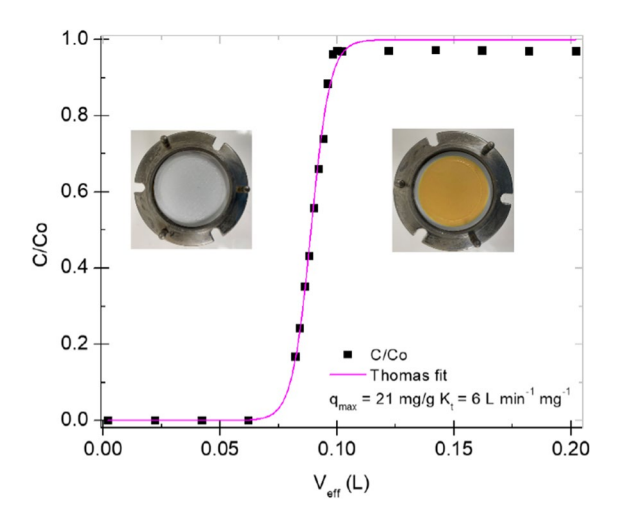


**Fig. 12** Breakthrough data for NaFL solution flowing through a CNR membrane. Relative analyte concentration is plotted versus analyte solution volume. The dynamic binding data are fitted to a Thomas model (line) to determine the  $K_T=6.0~L~min^{-1}~mg^{-1}$  and dynamic loading capacity  $q_{max}=20.8~mg/g$ . CNR film before (inset left) and after (inset right) NaFL adsorption

$$\frac{C}{C_o} = \left(1 + exp\left(K_T\left(q_{max}m - C_oV_{eff}\right)/Q\right)\right)^{-1}$$

and the maximum dynamic loading  $q_{max}$  and Thomas constant  $K_T$  are determined (Thomas 1944). The data in Fig. 12 are fitted by  $K_T = 6.0 \pm 0.3$  L min<sup>-1</sup> mg<sup>-1</sup> and  $q_{max} = 20.81 \pm 0.04$  mg/g. The similarity to the equilibrium  $q_{max} = 26.8 \pm 1.3$  mg/g is consistent with a brush-like "contact" ion-exchange resin action. The CNR mechanical integrity is illustrated in the before (left) and after (right insets in Fig. 12). The water flux of CNR after adsorbing NaFL was decreased to 707 L m<sup>-2</sup> h<sup>-1</sup> bar <sup>-1</sup>. Any pinholes or cracks in the film would result in an increased water flux.

Initial studies showed that CNR is effective at the removal of Perfluorooctane Sulfonate (PFOS) from water. The US EPA recently lowered its guidance on PFOS from 70 ppt to 0.004 ppt (USEPA 2022). Using direct injection electrospray ionization mass spectrometry (Velos Pro, Thermo Scientific), we measured PFOS concentrations in spiked DI water samples down to our limit of detection 100 ppt. Future studies will report PFOS removal using EPA Method 537.1 which will allow us to access the more stringent detection levels. Here, we present just the results

for the proof-of-concept. The experimental details are described in the electronic supplementary material section (Figures S11 and S12). We pushed 50.00 mL of a 1.00 ppb aqueous PFOS solution through a 100 µg CNR membrane film. The effluent PFOS concentration was measured after each mL of analyte pushed through the CNR. There was no detectable PFOS found in the effluent. This loading of 0.50 mg PFOS/g CNR is equivalent to purifying 500 L of water. Control studies that did not use CNR in the filter were detected at the 1.00 ppb level (no significant nonspecific binding). A series of aqueous PFOS solutions ranging from 1.00 ppb through 8.00 ppb was passed through the CNR. There was no detectable PFOS in the effluent.

CNR thin film regeneration and reuse was demonstrated using the surrogate binding analyte NaFL(aq). A film of 114 µg CNR was deposited onto a 0.2 µm MCE filter to make the nanoresin membrane. Then, 5.000 mL of 1.75 ppm NaFL (8.75 µg) was pushed through the membrane. This effluent concentration and volume were chosen to exceed the binding capacity of the membrane, where 77 mg FL<sup>-1</sup> per g CNR is ~three times larger than the equilibrium loading capacity detailed above. This was a dynamic adsorption taking only a couple of seconds. The effluent's absorbance at 491 nm was measured using UV-Vis spectroscopy. The measured absorbance of 0.290 was then used to calculate the concentration of the effluent 1.22 ppm. Subtracting the effluent concentration from the initial concentration yields the adsorbed mass of 2.65 µg onto 0.114 mg CNR, giving a loading capacity,  $q_e = 23.2$  mg NaFL per gram of CNR on the first use of the film. The membrane was then regenerated with aliquots of 4 M NaCl(aq) until the concentration of NaFL in the brined effluent was below our detection limit of 4 ppb (approximately 20 mL of 4 M NaCl(aq) was needed per cycle). DI water was passed through the membrane until the conductivity of the wash reached  $< 1 \mu S cm^{-1}$ . The process was repeated for a total of 40 cycles. Figure 13 shows the loading capacity, qe as a function of cycle number. A linear regression (dashed line) was used to model the efficiency loss per cycle of adsorption/regeneration. As shown in Fig. 13, the loading capacity of the CNR membrane decreased by  $-0.006 \pm 0.01$  mg/g per cycle. The material retained > 99% of its performance over 40 cycles. Even after several liters of water rinse, the material still performs the same as its initial



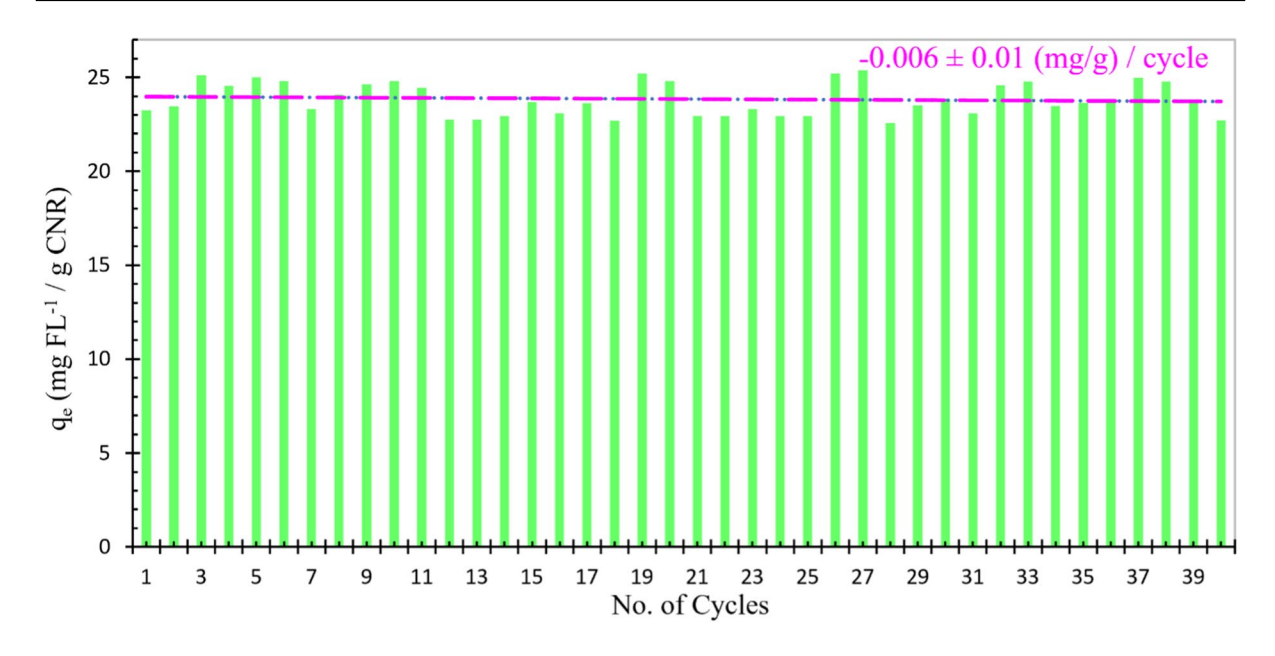


Fig. 13 CNR membrane regeneration and reuse. Loading capacity,  $q_e$  shown as a function of cycle number. Water purification thinfilm membrane performance decreased by  $0.006 \pm 0.01$  mg NaFL per gram of CNR through 40 cycles

loading. Since there is no perceivable degradation in performance, we conclude that this cellulose-based nanoresin is not decomposing, nor shedding polymer strands, and that all of the binding sites remain accessible to the analyte. These data suggest that CNR films, formed from the assemblies illustrated in Fig. 1, have high loading capacities and fast binding kinetics while simultaneously maintaining high water flux after many uses and regenerations. New materials like these enable a path towards a circular economy for water treatment methods and devices.

## **Conclusions**

Cellulose-based ion-exchange nanoresins have been synthesized in all-aqueous medium. Successful synthesis was confirmed by conductometric titration, DLS and zeta potential measurements. These materials consist of oxidized cellulose coupled to cationic polyelectrolyte strands. Cellulose was debundled by sonication and oxidized at the C-6 position of the D-glucose monomer via the TEMPO radical. Poly(vbTMAC) and CNR synthesis was achieved via ARGET-ATRP and acid-catalyzed Fischer-Speier esterification, respectively. We have shown that similar materials are capable of

removing several important anionic drinking water contaminants. Cellulose nanoresins will provide a more cost-effective alternative to our previous water purification materials (Johnson et al. 2016; Sahu et al. 2018, 2022) while maintaining high efficiency as adsorbent ion-exchange membranes. Our CNR materials exhibit high water flux of  $> 700 \text{ L m}^{-2} \text{ h}^{-1}$ bar  $^{-1}$ , high loading capacities of  $> 20 \text{ mg g}^{-1}$  when tested using NaFL surrogate adsorbate. In addition, we have shown fast adsorption kinetics, with equilibrium loading being achieved in a matter of seconds. Finally, successful regeneration was demonstrated over 40 cycles without significant performance loss. With our cellulose nanoresins, we hope to provide an affordable and sustainable material that is also an effective, efficient, and safe solution to the challenge of trace chemical contamination of drinking water.

Acknowledgments This material is based upon work supported by the National Science Foundation under Grant No. (2141056). This publication was developed under Assistance Agreement No. SV8408301 awarded by the U.S. Environmental Protection Agency to UNC Charlotte. It has not been formally reviewed by EPA. The views expressed in this document are solely those of UNC Charlotte and do not necessarily reflect those of the Agency. EPA does not endorse any products or commercial services mentioned in this publication.



**Author contributions** Material preparation, data collection and analysis were performed by all authors. The first draft of the manuscript was written by SCS and all authors commented on previous versions of the manuscript. All authors read and approved the final manuscript. Conceptualization: AS and JP; Methodology: AS, SS and JP; Formal analysis and investigation: RD, CK, AF, AS, SS and JP; Writing - original draft preparation: SS; Writing - review and editing: CK, AF, AS, SS and JP; Funding acquisition: AS and JP; Resources: JP; Supervision: JP.

**Funding** This material is based upon work supported by the National Science Foundation under Grant No. (2141056). This publication was developed under Assistance Agreement No. SV8408301 awarded by the U.S. Environmental Protection Agency to UNC Charlotte. It has not been formally reviewed by EPA. The views expressed in this document are solely those of UNC Charlotte and do not necessarily reflect those of the Agency. EPA does not endorse any products or commercial services mentioned in this publication.

#### **Declarations**

**Conflict of interest** The authors declare no competing interest.

**Human participants and animals** This research did not involve Human Participants and/or Animals.

**Informed consent** is not applicable for this work.

## References

- Abouzeid RE, Khiari R, El-Wakil N, Dufresne A (2019) Current state and new trends in the use of cellulose nanomaterials for wastewater treatment. Biomacromol 20(2):573–597. https://doi.org/10.1021/acs.biomac.8b00839
- Aburabie J, Lalia B, Hashaikeh R (2021) Proton conductive, low methanol crossover cellulose-based membranes. Membranes 11(7):539. https://doi.org/10.3390/membranes11070539
- Alston JR, Banks DJ, McNeill CX, Mitchell JB, Popov LD, Shcherbakov IN, Poler JC (2015) Adsorption studies of divalent, dinuclear coordination complexes as molecular spacers on SWCNTs. Phys Chem Chem Phys 17:29566– 29573. https://doi.org/10.1039/c5cp05419b
- Bampidis V, Azimonti G, Bastos MDL, Christensen H, Dusemund B, Kos Durjava M, Kouba M, López-Alonso M, López Puente S, Marcon F, Mayo B, Pechová A, Petkova M, Ramos F, Sanz Y, Villa RE, Woutersen R, Bories G, Gropp J, Nebbia C, Innocenti ML, Aquilina G (2020) Safety and efficacy of methyl cellulose for all animal species. EFSA J. https://doi.org/10.2903/j.efsa.2020.6212
- Calderón-Vergara LA, Ovalle-Serrano SA, Blanco-Tirado C, Combariza MY (2020) Influence of post-oxidation reactions on the physicochemical properties of TEMPOoxidized cellulose nanofibers before and after amidation. Cellulose 27(3):1273–1288. https://doi.org/10.1007/ s10570-019-02849-4

- Camarero Espinosa S, Kuhnt T, Foster EJ, Weder C (2013) Isolation of thermally stable cellulose nanocrystals by phosphoric acid Hydrolysis. Biomacromol 14(4):1223–1230. https://doi.org/10.1021/bm400219u
- Duan H, Shao Z, Zhao M, Zhou Z (2016) Preparation and properties of environmental-friendly coatings based on carboxymethyl cellulose nitrate ester & modified alkyd. Carbohydr Polym 137:92–99. https://doi.org/10.1016/j. carbpol.2015.10.067
- Geise GM, Lee H-S, Miller DJ, Freeman BD, McGrath JE, Paul DR (2010) Water purification by membranes: the role of polymer science. J Polym Sci Part B: Polym Phys 48(15):1685–1718. https://doi.org/10.1002/polb.22037
- Gurgel LVA, Perin de Melo JC, de Lena JC, Gil LF (2009)
  Adsorption of chromium (VI) ion from aqueous solution by succinylated mercerized cellulose functionalized with quaternary ammonium groups. Bioresour Technol 100(13):3214–3220. https://doi.org/10.1016/j.biortech. 2009.01.068
- Isogai A, Kato Y (1998) Preparation of polyuronic acid from cellulose by TEMPO-mediated oxidation. Cellulose 5(3):153–164. https://doi.org/10.1023/a:1009208603673
- Isogai A, Hänninen T, Fujisawa S, Saito T (2018) Review: catalytic oxidation of cellulose with nitroxyl radicals under aqueous conditions. Prog Polym Sci 86:122–148. https://doi.org/10.1016/j.progpolymsci.2018.07.007
- Ito H, Sakata M, Hongo C, Matsumoto T, Nishino T (2018) Cellulose nanofiber nanocomposites with aligned silver nanoparticles. Nanocomposites 4(4):167–177. https://doi. org/10.1080/20550324.2018.1556912
- Johnson BR, Eldred TB, Nguyen AT, Payne WM, Schmidt EE, Alansari AY, Amburgey JE, Poler JC (2016) Highcapacity and rapid removal of refractory NOM using nanoscale anion exchange resin. ACS Appl Mater Interfaces 8(28):18540–18549. https://doi.org/10.1021/acsami. 6b04368
- Jois HSS, Bhat DK (2013) Miscibility, water uptake, ion exchange capacity, conductivity and dielectric studies of poly(methyl methacrylate) and cellulose acetate blends. J Appl Polym Sci 130(5):3074–3081. https://doi.org/10. 1002/app.39535
- Juntadech T, Nantasenamat C, Chitpong N (2021) Oxidized regenerated cellulose nanofiber membranes for capturing heavy metals in aqueous solutions. Cellulose 28(18):11465–11482. https://doi.org/10.1007/s10570-021-04271-1
- Kalia S, Boufi S, Celli A, Kango S (2014) Nanofibrillated cellulose: surface modification and potential applications. Colloid Polym Sci 292(1):5–31. https://doi.org/10.1007/s00396-013-3112-9
- Kang X, Sun P, Kuga S, Wang C, Zhao Y, Wu M, Huang Y (2017) Thin cellulose nanofiber from corncob cellulose and its performance in transparent nanopaper. ACS Sustain Chem Eng 5(3):2529–2534. https://doi.org/10.1021/acssuschemeng.6b02867
- Klemm D, Schumann D, Kramer F, Heßler N, Hornung M, Schmauder H-P, Marsch S (2006) Nanocelluloses as Innovative Polymers in Research and Application. Springer, Berlin Heidelberg, pp 49–96
- Li Q, Chen G, Xing T, Miao S (2018) Dry transfer printing of silk and cotton with reactive dyes and mixed polysaccharide



- thickeners. Color Technol 134(3):222–229. https://doi.org/10.1111/cote.12337
- Lu H, Behm M, Leijonmarck S, Lindbergh G, Cornell A (2016) Flexible paper electrodes for Li-Ion batteries using low amount of TEMPO-oxidized cellulose nanofibrils as binder. ACS Appl Mater Interfaces 8(28):18097–18106. https://doi. org/10.1021/acsami.6b05016
- Luneva NK, Ezovitova TI (2014) Cellulose phosphorylation with a mixture of orthophosphoric acid and ammonium polyphosphate in urea medium. Russ J Appl Chem 87(10):1558–1565. https://doi.org/10.1134/s107042721 4100243
- Luo W, Shen F, Bommier C, Zhu H, Ji X, Hu L (2016) Na-Ion battery anodes: materials and electrochemistry. Acc Chem Res 49(2):231–240. https://doi.org/10.1021/acs.accounts. 5b00482
- Matyjaszewski K, Dong H, Jakubowski W, Pietrasik J, Kusumo A (2007) Grafting from surfaces for everyone: ARGET ATRP in the presence of air. Langmuir 23(8):4528–4531. https://doi.org/10.1021/la063402e
- Morits M, McKee JR, Majoinen J, Malho J-M, Houbenov N, Seitsonen J, Laine J, Gröschel AH, Ikkala O (2017) Polymer brushes on cellulose nanofibers: modification, SI-ATRP, and unexpected degradation processes. ACS Sustain Chem Eng 5(9):7642–7650. https://doi.org/10.1021/acssuschem eng.7b00972
- Nair N, Kim W-J, Braatz RD, Strano MS (2008) Dynamics of surfactant-suspended single-walled carbon nanotubes in a centrifugal field. Langmuir 24(5):1790–1795. https://doi. org/10.1021/la702516u
- Nguyen H, Hsiao M-Y, Nagai K, Lin H (2020) Suppressed crystallization and enhanced gas permeability in thin films of cellulose acetate blends. Polymer 205:122790. https://doi.org/10.1016/j.polymer.2020.122790
- Nikiforova TE, Kozlov VA (2011) Study of the effect of oxidative-bisulfite modification of the cotton cellulose on its ion exchange properties. Russ J Gen Chem 81(10):2136–2141. https://doi.org/10.1134/s1070363211100173
- O'Connell DW, Birkinshaw C, O'Dwyer TF (2008) Heavy metal adsorbents prepared from the modification of cellulose: a review. Bioresour Technol 99(15):6709–6724. https://doi.org/10.1016/j.biortech.2008.01.036
- Obele CM, Ibenta ME, Chukwuneke JL, Nwanonenyi SC (2021) Carboxymethyl cellulose and cellulose nanocrystals from cassava stem as thickeners in reactive printing of cotton. Cellulose 28(4):2615–2633. https://doi.org/10.1007/ s10570-021-03694-0
- Perinelli DR, Berardi A, Bisharat L, Cambriani A, Ganzetti R, Bonacucina G, Cespi M, Palmieri GF (2021) Rheological properties of cellulosic thickeners in hydro-alcoholic media: the science behind the formulation of hand sanitizer gels. Int J Pharm 604:120769. https://doi.org/10.1016/j.ijpharm. 2021 120769
- Sahu A, Blackburn K, Durkin K, Eldred TB, Johnson BR, Sheikh R, Amburgey JE, Poler JC (2018) Green synthesis of nanoscale anion exchange resin for sustainable water purification. Environ Sci Water Res Technol 4(10):1685–1694. https://doi.org/10.1039/C8EW00593A
- Sahu A, Sheikh R, Poler JC (2020) Green sonochemical synthesis, kinetics and functionalization of nanoscale anion exchange resins and their performance as water purification

- membranes. Ultrason Sonochem 67:105163. https://doi.org/10.1016/j.ultsonch.2020.105163
- Sahu A, Alston JR, Carlin C, Craps M, Davis K, Harrison HB, Kongruengkit T, Manikonda A, Elmore S, Rollins R, Sadiku B, Schmal S, Shajahan J, Poler JC (2022) Fluorographite nanoplatelets with covalent grafting of anion-exchange resins for water purification. ACS Appl Nano Mater. https:// doi.org/10.1021/acsanm.2c00709
- Sahu A, Dosi R, Kwiatkowski C, Schmal S, Poler JC (2023) Advanced polymeric nanocomposite membranes for water and wastewater treatment: a comprehensive review. Polymers 15(3):540
- Sèbe G, Ham-Pichavant F, Pecastaings G (2013) Dispersibility and emulsion-stabilizing effect of cellulose nanowhiskers esterified by vinyl acetate and vinyl cinnamate. Biomacromol 14(8):2937–2944. https://doi.org/10.1021/bm400854n
- Sharma A, Anjana, Rana H, Goswami S (2021) A comprehensive review on the heavy metal removal for water remediation by the application of lignocellulosic biomass-derived nanocellulose. J Polym Environ. https://doi.org/10.1007/s10924-021-02185-4
- Shibata I (2003) Depolymerization of cellouronic acid during TEMPO-mediated oxidation. Cellulose 10(2):151–158. https://doi.org/10.1023/a:1024051514026
- Singh N, Wang J, Ulbricht M, Wickramasinghe SR, Husson SM (2008) Surface-initiated atom transfer radical polymerization: a new method for preparation of polymeric membrane adsorbers. J Membr Sci 309(1–2):64–72. https://doi.org/10. 1016/j.memsci.2007.10.007
- Spinella S, Maiorana A, Qian Q, Dawson NJ, Hepworth V, McCallum SA, Ganesh M, Singer KD, Gross RA (2016) Concurrent cellulose hydrolysis and esterification to prepare a surface-modified cellulose nanocrystal decorated with carboxylic acid moieties. ACS Sustain Chem Eng 4(3):1538– 1550. https://doi.org/10.1021/acssuschemeng.5b01489
- Thomas HC (1944) Heterogeneous ion exchange in a flowing system. J Am Chem Soc 66(10):1664–1666. https://doi.org/10.1021/ja01238a017
- USEPA (2022) Proposed designation of perfluorooctanoic acid (PFOA) and perfluorooctanesulfonic acid (PFOS) as CER-CLA hazardous substances. Available online: https://www.govinfo.gov/content/pkg/FR-2022-09-06/pdf/2022-18657.pdf [Accessed]
- Yoshikawa C, Sakakibara K, Nonsuwan P, Shobo M, Yuan X, Matsumura K (2022) Cellular flocculation driven by concentrated polymer brush-modified cellulose nanofibers with different surface charges. Biomacromol 23(8):3186–3197. https://doi.org/10.1021/acs.biomac.2c00294
- **Publisher's Note** Springer Nature remains neutral with regard to jurisdictional claims in published maps and institutional affiliations.

Springer Nature or its licensor (e.g. a society or other partner) holds exclusive rights to this article under a publishing agreement with the author(s) or other rightsholder(s); author self-archiving of the accepted manuscript version of this article is solely governed by the terms of such publishing agreement and applicable law.

